Analysis of the Complex z-Plane Fractal Images from $z \leftarrow z^{-\alpha} + c$ for $\alpha > 0$

by

S.V. Dhurandhar, V.C. Bhavsar and U.G. Gujar

TR90-055, September 1990

Faculty of Computer Science
University of New Brunswick
P.O. Box 4400
Fredericton, N.B. E3B 5A3

Phone: (506) 453-4566
Fax: (506) 453-3566

Analysis of the complex z-plane Fractal Images

from $z \leftarrow z^{-\alpha} + c$ for $\alpha > 0$.

Sanjeev V. Dhurandhar
Inter University Centre for Astronomy and Astrophysics
Poona University Campus, Ganeshkhind,
Pune 411 007, INDIA

Virendra C. Bhavsar and Uday G. Gujar
Faculty of Computer Science
University of New Brunswick,
Fredericton, N.B., E3B 5A3, CANADA

ABSTRACT

The z-plane fractal images generated from the generalized transformation function $z \leftarrow z^{-\alpha} + c,\ \alpha > 0$, are analyzed. The fractal images appear to be planetary structures with a central planet surrounded by satellite structures. The positions and the sizes of the planet and satellite structures are analytically estimated. The partial structures arising for non-integer values of α are analysed. For α greater than a critical value drastic changes occur in the images and these changes are explained.

Keywords: *Fractals, Dynamical Systems, Complex Analysis.*

1. Introduction

The fractals generated from the self-squared function, $z \leftarrow z^2 + c$, where z and c are complex quantities, have been studied extensively in the literature [MAND 82, PEIT 86]. Recently, the generalized transformation function, $z \leftarrow z^\alpha + c$, for positive integer values of, has been considered in [LAKH 87] and α-fold symmetries have been observed in the resulting fractal images. The c- plane fractals from this function for integer and real values of α, α being positive or negative, have been dealt in [GUJA 90a]. The z-plane fractal images from this function have been presented in [GUJA 90b] along with some conjectures about their visual characteristics. In this paper, we consider the transformation $z \leftarrow z^{-\alpha} + c$, for $\alpha > 0$, and analyse the z-plane fractal images generated from the iterations of this function proving all of the conjectures for $\alpha > 0$ given in [GUJA 90b]. In addition several new visual characteristics are mathematically explained.

2. Preliminaries

The process of generating fractal images from $z \leftarrow z^{-\alpha} + c$ is given in detail in [GUJA 90a] and is similar to the one employed for the self-squared function [PEIT 86]. Briefly, this process consists of iterating this function upto N times. Starting from a value z_o, we obtain $z_1, z_2, \ldots$ by applying the transformation $z_{n+1} \leftarrow z_n^{-\alpha} + c$. We color the point z_o with a color m if $|z_m| \geq L$ and $|z_p| < L$ for $p < m$; the quantity L is called the preset limit. Thus, a fractal image consists of a set of colored pixels in complex z-plane. The generalized transformation function is multi-valued with finite or infinite branches and corresponding Riemann sheets [AHLF 85]. Consequently, this gives rise to rich structures studied in this paper.

Several fractal images have been generated by using $z \rightarrow z^{-\alpha} + c$ in the complex z-plane, where $\alpha > 0$ and c is a complex constant. For all the fractal images presented in this paper, number of pixels equal 360×360, $N = 100$, $L = 10$, $|\ Re(z)| \leq 1.5$ and $|Im(z)| \leq 1.5$ unless otherwise specified. Further, a pixel is colored white if $|z| < L$ for all

N iterations and we say that such a pixel belongs to the stable region, otherwise the pixel is part of an unstable region colored non-white. Ideally (mathematically), the stable and unstable regions are derived as above in the limit $N \to \infty$.

For the purposes of analysis of the fractal images from $z \leftarrow z^{-\alpha}+c$, $\alpha > 0$, we consider the following cases based on the quantitative features of the images:

(i) Integer α
(ii) Noninteger α
(iii) The phase transition at $\alpha = \alpha_p$, and
(iv) Beyond phase transition $\alpha > \alpha_p$,

where α_p is a critical value of α to be defined later in the text.

3. Integer α

Figure 1 shows fractal images generated for $\alpha = 4$ and $\alpha = 6$. These images resemble planetary structures with a central planet surrounded by satellite structures. The number of major satellite structures is equal to α and are situated symmetrically around the origin. We also observe that the unstable regions are embedded in the stable region.

3.1 The Central Planet

We have observed that for integer values of α there exists one near-circular central planet symmetric around the origin. Some properties of this central planet are established below.

Theorem 1: The fractal image from the transformation $z \leftarrow z^{-\alpha} + c$ consists of a central planet which has a near-circular shape with the origin as its center and its radius $\simeq L^{-1/\alpha}$. The deviations from the circular shape have α-fold symmetry.

Proof: The central planet arises when $|z|$ becomes greater than L immediately after the first iteration (i.e. $n = 1$). This is clear from the fact that the origin gets mapped to

infinity (i.e. greater than L) under $z \leftarrow z^{-\alpha} + c$. Hence by continuity some neighborhood of the origin gets mapped to the neighborhood of infinity $|z| > L$. This establishes that the neighborhood around the origin arises after the first iteration.

The size of the central planet is found as follows. Let

$$z_1 \leftarrow z_0^{-\alpha} + c, \text{ and}$$

$$z_0 = re^{i\theta}, \; c = |c|e^{i\phi}$$

We have to find those z_0 's for which $|z_1| \geq L$.

$$\begin{aligned} z_1 &= \frac{1}{z_0^{\alpha}} + c \\ &= \frac{1}{r^{\alpha}} e^{-i\alpha\theta} \quad + |c|e^{i\phi} \end{aligned} \tag{3.1}$$

For $|c| \ll L$, we neglect c in the first approximation and taking modulus of the above equation we obtain

$$|z_1| = \frac{1}{r^{\alpha}} \geq L.$$

Therefore,

$$r \leq L^{-1/\alpha}. \tag{3.2}$$

The equation also applies to non-integer values of α.

The deviations to the circular shape of the central planet can be obtained as follows. Taking the modulus square of the Eq.(3.1) we obtain,

$$|z_1|^2 = r^{-2\alpha} + 2r^{-\alpha}|c|cos(\alpha\theta + \phi) + |c|^2. \tag{3.3}$$

If $|z_1|^2 \geq L^2$, we can solve Eq. (3.3) for r as a function of θ. We solve this equation for the case when $|c| \ll L$. Since the deviations are small from circularity [see Eq. (3.2)] we write

$$r(\theta) = L^{-1/\alpha}(1 + \delta(\theta)) \tag{3.4}$$

where $\delta(\theta) \ll 1$.

Substituting Eq. (3.4) into Eq. (3.3) and keeping only the first-order terms in the equation we get

$$\delta(\theta) \simeq \frac{1}{L} \cdot \frac{|c|}{\alpha} cos(\alpha\theta + \phi). \tag{3.5}$$

Thus the deviations have α-fold symmetry.

Remarks: The Theorem 1 is illustrated for $\alpha = 4$, $c = 0.5 + i0.5$ and $L = 10$. The radius of the central planet is approximately

$$r \simeq L^{-1/4} = 0.56234$$

The maximum radial deviation is given by,

$$\delta_{max} \simeq \frac{1}{10} \times \frac{1}{\sqrt{2} \times 4} = 0.01768$$

which occurs at

$$\left(4\theta + \frac{\pi}{4}\right) = 0,\ 2\pi,\ 4\pi \text{ and } 6\pi.$$

Thus

$$\theta = \frac{-\pi}{16},\ \frac{7\pi}{16},\ \frac{15\pi}{16} \text{ and } \frac{23\pi}{16}.$$

Further, as α increases the radius $L^{-1/\alpha}$ of the central planet also increases as clearly seen in Figure 1. In fact, for large α this radius is approximately equal to one.

The images in Figure 1 consist of several circular blobs. As shown in Theorem 1, the central blob (planet) arises after the first iteration. We denote it by B^1. Similarly, the blobs (satellite structures) arising from the $k - th$ iteration will be denoted by B^k. B^k consists of those z_0 points for which $|z_k| \geq L$ and $|z_m| < L$ for $m < k$.

3.2 The major satellite structures (B^2 blobs)

As stated earlier, the number of major satellite structures, i.e. the circular blobs just smaller than the planet, equals α. We show that these structures result from the second

iteration ($n = 2$) i.e. they are B^2 blobs. The pixels which belong to B^2 arise due to the following. The first iteration for the pixels maps them to the central planet B^1 and in the next interation, these pixels map into the region $|z| \geq L$. Alternatively, the B^2 blobs can be looked upon as preimages – images under the inverse mapping $z \leftarrow (z-c)^{-1/\alpha}$ – of the B^1 blob. Since the inverse mapping is multivalued with α branches, it gives rise to α satellites.

Theorem 2: The B^2 blobs exist only when c lies outside the B^1 region and then their number equals α. These blobs are situated more or less symmetrically about the points $(-c)^{-1/\alpha}$. The angular size Ω, i.e. the angle subtended by blob at the origin, is given by $\frac{2}{\alpha} sin^{-1}\left\{\frac{L^{-1/\alpha}}{|c|}\right\}$.

Proof: The pixels which belong to B^2 are clearly the preimages of the B^1 pixels. The inverse mapping is

$$z_0 = (z_1 - c)^{-1/\alpha} \tag{3.6}$$

and if $z_1 \epsilon B^1$ then $z_0 \epsilon B^2$.

Since the origin $z = 0$ belongs to B^1, from Eq. (3.6),

$$z_0 = (-c)^{-1/\alpha} \tag{3.7}$$

belongs to B^2. This equation has α roots which represent the centres of the B^2 blobs. Since $c \notin B^1$, the Eq. (3.6) has always non-singular roots and thus gives rise to these blobs.

The angular size of the B^2 blobs is estimated by the following geometrical construction in the complex plane. Let Ω be the angular diameter of a B^2 blob and consider the inverse mapping in Eq. (3.6) with $z_1 \in B^1$.

Now Ω is the difference between the maximum and the minimum values of the argument of z_0 as z_1 varies over B^1. Consider the complex number $w_1 = z_1 - c$; w_1 is obtained from z_1 by shifting the origin to c, i.e. w_1 is a vector drawn from c to z_1. We wish to find out the difference Δ between the maximum and the minimum arguments of w_1 as z_1 varies over B^1. These values of w_1 are obtained by drawing tangents from c to B^1.

The two values of z_1 at which the tangents touch B^1 give the required values. Assuming B^1 to be a circle with radius $(L^{-1/\alpha})$ and center $z = 0$, elementary geometry gives $\Delta = 2sin^{-1}\left\{\frac{L^{-1/\alpha}}{|c|}\right\}$ which immediately implies from the inverse mapping that

$$\Omega = \frac{2}{\alpha} sin^{-1}\left\{\frac{L^{-1/\alpha}}{|c|}\right\}.$$

Since the center of a B^2 blob is situated at $(-c)^{-1/\alpha}$, the radial distance of its center from the origin is $|c|^{-1/\alpha}$ and has the linear diameter D given by

$$D \simeq \frac{2}{\alpha |c|^{1/\alpha}} sin^{-1}\left\{\frac{L^{-1/\alpha}}{|c|}\right\}.$$

Remarks: For $\alpha = 4$ and $c = 0.5 + i\ 0.5$ and $L = 10$, $\Omega = 26.34^0$ and the linear diameter $D = 0.5014$.

For higher values of α, e.g. $\alpha = 6$, the B^2 blobs get elongated. This can be explained as follows. As α increases, the size of the B^1 blob increases resulting into decrease in the distance between c and B^1. With the use of inverse mapping, a point of B^1 closest to c gets mapped further away from the origin resulting in the elongation.

3.3 Other Satellite Structures (B^k, $k \geq 3$)

Figure 1 shows many minor satellite structures forming a necklace around the central planet. Now we consider the properties of these satellite structures.

These satellite structures are generated by higher number iterations. A $k - th$ order satellite structure is defined by

$$B^k = \left\{z_0 / |z_k| \geq L \; and \; |z_m| < L \; for \; \forall m < k\right\}.$$

The B^k can be defined recursively through the inverse mapping as follows.

Let $f\ :\ z \leftarrow z^{-\alpha} + c$. Then,

$$B^k = \underbrace{f^{-1} \circ f^{-1} \ldots \circ f^{-1}}_{k \text{ times}} \{z | z| \geq L\}$$
$$= \underbrace{f^{-1} \circ \ldots \circ f^{-1}}_{(k-1) \text{ times}} \{B^1\}$$
$$= \underbrace{f^{-1} \circ \ldots \circ f^{-1}}_{(k-q) \text{ times}} \{B^2\}$$

f^{-1} is α-valued and the repeated application of f^{-1} produces $\alpha^{(k-1)}$ number of B^k blobs. In the case of $\alpha = 4$, for example, there are four B^2 blobs.

Therefore the unstable region is

$$U = \bigcup_{k=1}^{\infty} B^k,$$

i.e. for any $z_0 \in U$ there exists m such that $|z_m| \geq L$. In contrast there is a stable region S, colored white, where the successive interations of the function get trapped into cycles wherein $|z| < L$. The boundary between the regions S and U is the fractal where a point on the boundary cannot decide whether to remain bounded or otherwise.

The B^3 blobs are obtained from the relation Eq. (3.6) where $z_0 \in B^3$ if $z_1 \in B^2$. The angular sizes of B^3 blobs can be obtained by following the discussion in Section 3.2, i.e. constructing tangents from c to the B^2 blobs. This, in general, gives rise to smaller structures and their size decreases as k increases. The positions of these blobs can be identified with their approximate centers. The center of a B^3 blob gets mapped to the center of same B^2 blob which further gets mapped to the center of B^1 blob (which is the origin). Thus, centers of the α^2 number of B^3 blobs are given by the roots of

$$\left((-c)^{-1/\alpha} - c\right)^{-1/\alpha}.$$

Similarly, the centers of α^3 number of B^4 blobs are given by the roots of

$$\left((-c)^{-1/\alpha} - c)^{-1/\alpha} - c\right)^{-1/\alpha}.$$

The formula can be extended in an obvious manner for finding the centers of higher order satellite structures. It should be noted that the centers of the blobs depend only the values of c and α and their sizes are determined also by L.

4. Non-Integer α

Figure 2 shows three images for fractional powers $\alpha = 4.2$, $\alpha = 4.5$ and $\alpha = 4.8$. Figure 2(a) does not have a partial B^2 blob, although there exists notable partial B^3 blob. In Figure 2 (b), a partial B^2 blob is seen to emerge over the negative real axis, whereas the partial B^3 blob is now fully grown. In the last image in Figure 2, the partial B^2 blob has grown in size; it was found that for $\alpha = 5$, this partial blob gets completed.

The existence of partial blobs can be explained as follows. In computing the iterations of $z \leftarrow z^{-\alpha} + c$, the arguments of the complex quantities get multiplied by α. However, the arguments have to be restricted to some interval of length 2π; this interval is usually chosen $-\pi$ to π or 0 to 2π. The multiplication of an argument of a complex quantity by α can make its value go beyond this range and in this case the complex quantity will have its argument modified by $\pm 2\pi$ which results in a discontinuity exhibited by the cutting of the blobs.

It should be noted that the partial blobs occur only when α is non-integer. This is due to the following. If we assume that the argument of a complex number lies between $-\pi$ to π, there is a discontinuity in the argument as the negative real axis is crossed by the complex number. The function $z \leftarrow z^{-\alpha} + c$ at the negative real axis is continuous or discontinuous according as α is an integer or a noninteger, respectively. For example, let,

$$z = e^{i\pi} = e^{-i\pi}$$

then,

$$w_1 = z^{-\alpha} = e^{-i\pi\alpha} \text{ and } w_2 = z^{-\alpha} = e^{i\pi\alpha}.$$

For α an integer, $w_1 = w_2$, whereas for non-integer α, $w_1 \neq w_2$.

Now consider the B^2 blobs and Theorem 2. It is easily seen that for a non-integer value of α, the discussion in Theorem 2 applies for finding the maximum and minimum angular limits for a full B^2 blob. The angular position of the centre of a B^2 blob is given by $-\frac{1}{\alpha}(\pi + \phi)$, ϕ being the argument of c. Therefore, these limits denoted by θ^+ and θ^- respectively, are given as,

$$\theta^{\pm} = -\frac{1}{\alpha}(\pi + \phi) \pm \frac{\Omega}{2}.$$

The rest of blobs are obtained by rotations of this blob through multiples of $\frac{2\pi}{\alpha}$, both in clockwise and anticlockwise directions with the condition that a blob is not allowed to cross the negative real axis, for the case of generating the images given in Figure 2. (This implicitly assumes that the argument of z lies in the range $-\pi$ to π.) Consequently, if a blob happens to partially cross the negative real axis in either direction (above or below) the part of a blob which would have crossed the negative real axis disappears. More specifically, if for some positive integers m and m'

(a) $\theta^{+} + \frac{2\pi m}{\alpha} > \pi > \theta^{-} + \frac{2\pi m}{\alpha}$, or

(b) $\theta^{-} - \frac{2\pi m'}{\alpha} < -\pi < \theta^{+} - \frac{2\pi m'}{\alpha}$,

then a partial blob results. In case (a), the partial blob exists above the negative real axis upto $(\theta^{-} + \frac{2\pi m}{\alpha})$, whereas in case (b), the partial blob appears below the negative real axis upto $(\theta^{+} - \frac{2\pi m'}{\alpha})$.

A partial B^2 blob will give rise to an infinite hierarchy of partial B^k blobs, $k > 2$, which are successive preimages of the partial B^2 blob. The partial blobs can emerge at arbitrary iterations, $n > 1$. Figure 2 (a) shows that there is no partial B^2 blob at the same time there exists a partial B^3 blob. The root of a hierarchy of partial structures is always positioned on the negative real axis since the argument of a complex quantity is discontinuous here as assumed.

We illustrate the above discussion for the case of $\alpha = 4.5$. In this case, $\phi = 45°$ and $\frac{\Omega}{2} = 12.88°$. This gives for a B^2 blob $\theta^{+} = -37.12°$ and $\theta^{-} = -62.88°$. The other B^2 blobs are obtained by rotation through the angle $\frac{2\pi}{\alpha} = 80.00°$. Thus, the angular spans of the other B^2 blobs will be : (17.12°, 42.88°), (97.12°, 122.88°), (177.12°, 202.88°), (−142.88°, −117.12°) and (−222.88°, −197.12°). Since the angles are measured from −180° to +180°, the B^2 blob with the range (202.88°, 177.12°) appears partial with the range (180°, 177.12°) as clearly seen in the Figure 2(c). However,, the B^2 blob for the range (−222.88°, −197.12°) does not appear at all. The rest of the B^2 blobs being in the valid range appear as full.

5. Phase Transition

Figure 3 shows a fractal image obtained for $\alpha = 6.5$. We observe that there is a drastic change in the patterns for the regions arising for iterations with $n > 1$, as seen for the regions outside the central planet (i.e. B^1 blob). The B^1 blob has a larger size (as proven in Theorem 1) compared to the image for $\alpha = 6$ (see Figure 1(b)). The stable region (white color) for images in Figure 1 and 2 surrounds all the blobs and extends to infinity. This follows from the fact that the far away points get mapped near the point c which lies in the stable region, and hence they belong to the stable region.

In contrast, in Figure 3, the unstable region seems to extend to infinity while the stable region is bounded around the central planet. Further, the minor satellite structures form connected sets in contrast to the images in Figure 1 and 2. We can explain this phenomena as follows.

Firstly, the central planet grows in size, with radius $\simeq L^{-1/\alpha}$, as the value of α is increased and secondly, the minor satellite structures are pulled closer to the central planet. Thus it is plausible that the point c will get engulfed for some value of α, say $\alpha = \alpha_p$, by some B^k, $k < N$. As soon as this happens, for the subsequent iteration, k+1, all the points which correspond to the larger values of z belong to B^{k+1}, which is the unstable region. Thus resulting into a bounded stable region.

We now estimate the upper bound on the value of α_p. This can be achieved by noting the value of α for which the central planet engulfs point c. Since the central planet has radius $\simeq L^{-1/\alpha}$, for large α, this radius tends to 1. Therefore, our estimate is valid when $|c| < 1$. The value α, α_1, at which the point c lies on the boundary of the central planet is given approximately by the equation

$$L^{-1/\alpha_1} = |c|.$$

It should be noted that $\alpha_p \leq \alpha_1$. For Figure 3, $c = 0.5 + i0.5$ which gives $\alpha_1 = 6.64$. In this figure the phase transition has already occurred because the point c is engulfed by the minor satellite structures (resulting for $n > 1$). Since the size of the minor satellite structures in small, α_1 and α_p are close.

6. Beyond Phase Transition

When the value of α is increased beyond $\alpha = \alpha_p$, we obtain images similar to the one shown in Figure 4 for $\alpha = 9$. This image is quite different than the images obtained for $\alpha < 6.5$ and it is little different than that for $\alpha = 6.5$. The B^2 "blobs" have merged together to form a connected region which extends to infinity and surrounds the inner structures, including the stable region. The central planet size has further increased and has definitely engulfed c since $\alpha > \alpha_1$. The region surrounding the B^1 blob is the annular B^3 "blob" whereas the region providing the inner lining to the B^2 region corresponds to the B^4 region. These visual features can be explained mathematically as follows.

Since the explanation of the B^1 region is the same as in the earlier sections, first we consider the B^2 regions. Consider a point z_0, with $|z_0| \to \infty$. Then

$$z_1 = z_0^{-9} + c \simeq c.$$

Since $c \in B^1$, $z_1 \in B^1$ and hence $z_0 \in B^2$. Therefore a neighborhood of infinity gets mapped first inside the central planet and a further iteration throws it outside $|z| \leq L$.

The region just outside B^1 is B^3 region because this region by the first iteration gets mapped just inside the circle $|z| = L$ which is the B^2 region. Hence this region is B^3. Further, the inner lining of the B^2 region gets mapped to the B^3 region which is just outside the B^1 region. This shows that this region is the B^4 region. Thus we argue that the regions generated by the regions for the odd iterations keeps on growing outwards as the, order of the iteration increases, whereas the region resulting from the collection of even numbered iterations grows inwards. The stable region is trapped between these two regions and there the fractal results. This behavior is a consequence of the fact that the exponent for z is a negative quantity which makes the sequence z_0, z_1,..., oscillate.

7. Conclusion

In this paper, we have considered the generalized transformation function $z \leftarrow z^{-\alpha} +$

c, $\alpha > 0$, and mathematically analyzed the visual characteristics of the fractal images in the complex z-plane. For this function two classes of fractal images result depending on whether the value of α is less than some critical value α_p or not. For $\alpha < \alpha_p$, the fractal image consists of planetary structures which are the unstable regions, embedded in a stable region. We have estimated analytically the sizes and positions of the central planet and many of the satellite structures. For fractional values of α, we have explained the appearance of partial satellite structures. For $\alpha > \alpha_p$, the drastic change in the images is shown to arise due to the engulfing of the point c by planet and or satellite structures. The images in this case consist of an annular bounded stable region trapped between two unstable regions.

Although we have carried out interesting analysis of some visual characteristics of the fractal images, there are many unexplored and unexplained areas and we believe that voluminous work can be carried out for $z \leftarrow z^{\alpha} + c$ function on similar lines as has been carried out by earlier investigators for the case $\alpha = 2$.

Acknowledgements

This work germinated during the first workshop on *High Performance Computing,* March 1–4, 1990, organized by the center for Development of Advanced Computing (C-DAC), Pune, India. The work has been carried out during the sabbatical leave of one of us (VCB) from the University of New Brunswick at C-DAC, Pune. The partial support from the research grant OGP 0089 from the Natural Sciences and Engineering Council of Canada held by VCB is gratefully acknowledged.

References

[AHLF85] Lars V. Ahltors, *Complex Analysis : An Introduction to the Theory of Analytic Functions of One Complex Variable*, Mc Graw Hill, Auckland, 1985.

[GUJA90a] Gujar, U.G., Bhavsar, V.C., *Fractal Images from $z \leftarrow z^{\alpha} + c$ in complex c-plane*, Computers and Graphics, Vol. 14, No. 2, 1990 (to appear).

[GUJA90b] Gujar, U.G., Bhavsar, V.C. and N. Vangala, *Fractal Images from $z \leftarrow z^{\alpha} + c$ in the complex z-plane*, Internal Report, Faculty of Computer Science, University of New Brunswick, Fredricton, Canada, Internal Report, May 1990.

[LAKH87] Lakhtakia, A., Varadan, V.V., Messier, R., and Varadan, V.K., *On the Symmetries of the Julia Sets for the Process $z \Longrightarrow z^p + c$*,, J. Phy. A : Math. Gen, Vol. 20, pp. 3533-3535, 1987.

[MAND82] Mandelbrot, B.B., *The Fractal Geometry of Nature*, W.H. Freeman Company, San Fransisco, CA, 1982.

[PEIT86] Peitgen, H.O. and Richter, P., *The Beauty of Fractals*, Springer-Verlag, Berlin, 1986.

Figure Captions

1. Fractal images for integer α.
   (a) $\alpha = 4$ (b) $\alpha = 6$.
2. Fractal images for non-integer α.
   (a) $\alpha = 4.2$ (b) $\alpha = 4.5$ (c) $\alpha = 4.8$.
3. Phase transition $\alpha = 6.5$.
4. Beyond the phase transition $\alpha = 9$.

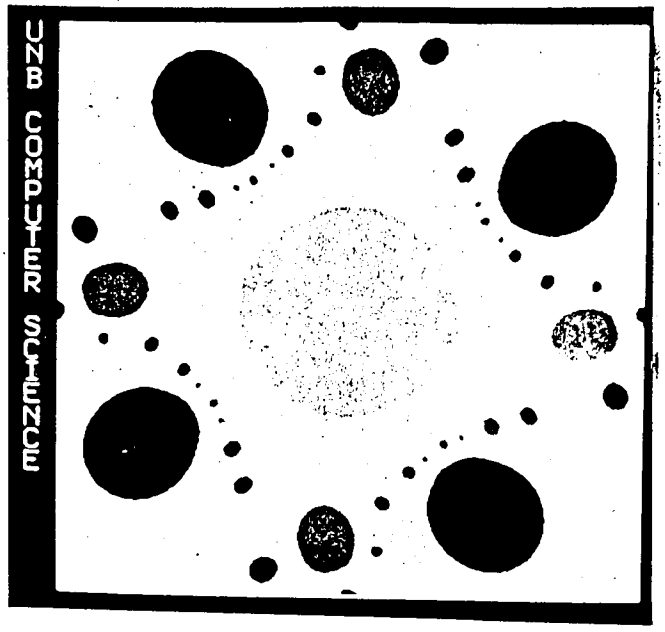

Figure 1(a)

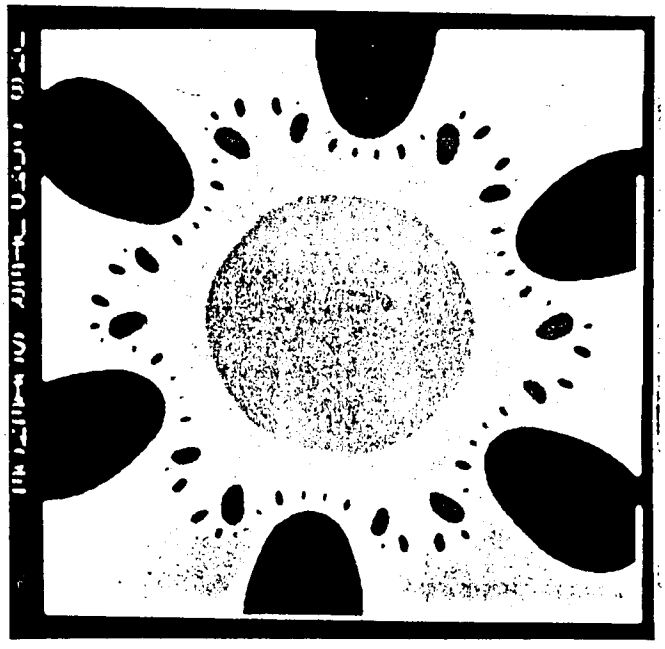

Figure 1(b)

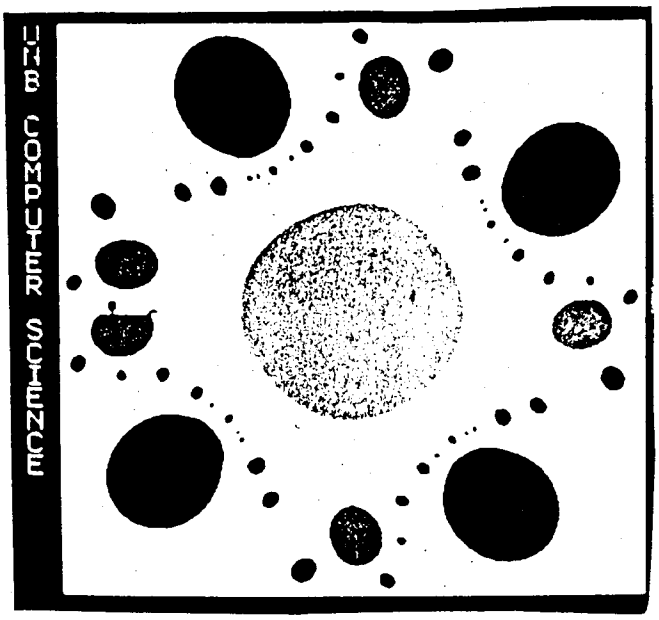

Figure 2(a)

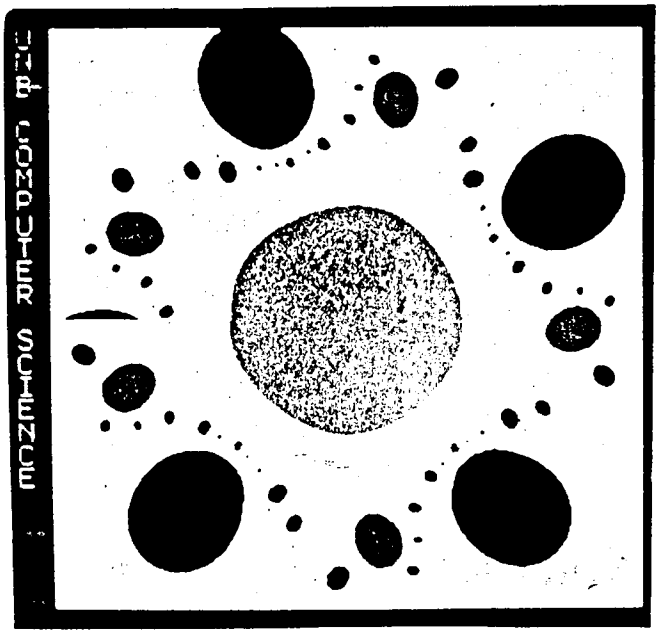

Figure 2(b)

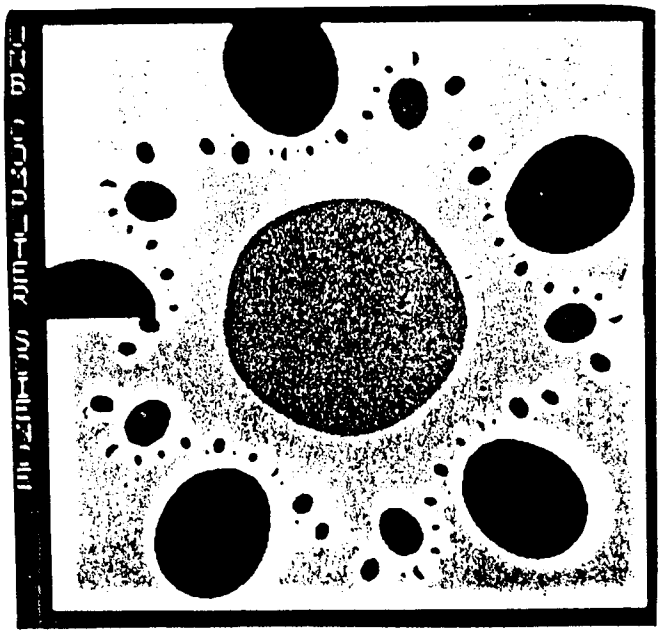

Figure 2(c)

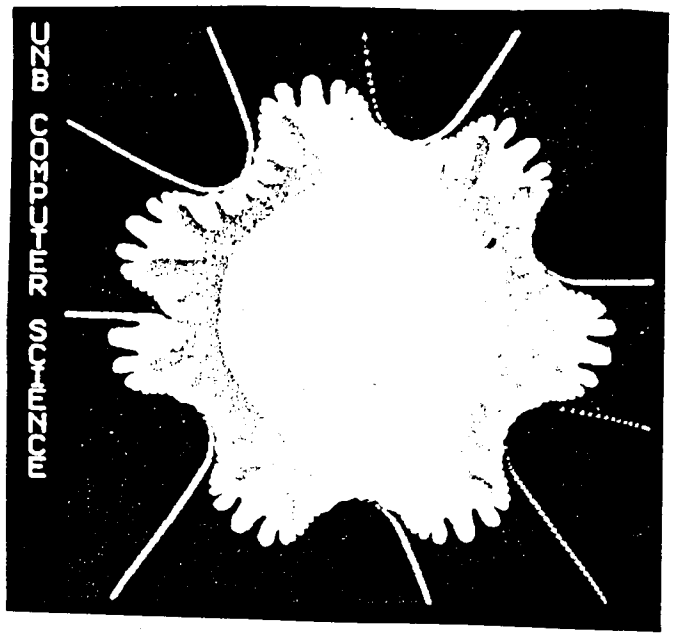

Figure 3

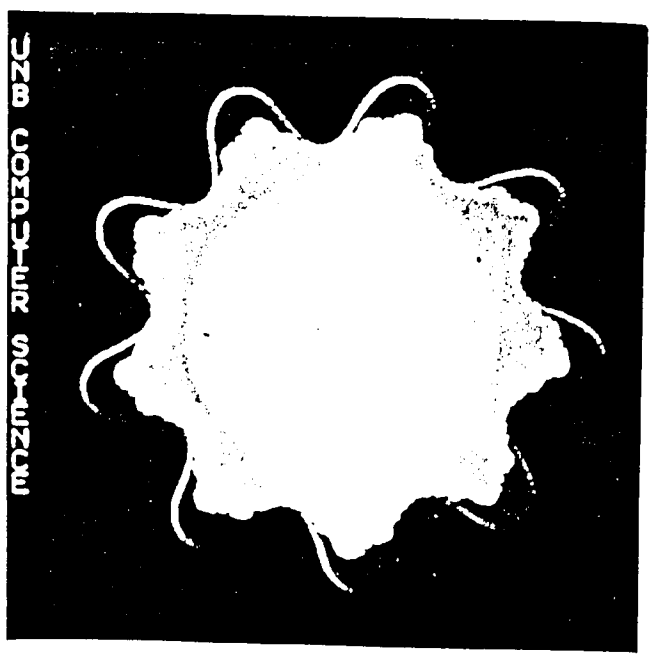

Figure 4